A Curious Artifact in the Potential Energy Surface for the F + HF Abstraction Reaction

Gary L. Fox† and H. B. Schlegel*

Contribution from the Department of Chemistry, Wayne State University, Detroit, Michigan 48202

Received October 26, 1992

Abstract: The reaction F + HF → HF + F has been studied using ab initio molecular orbital theory at UHF, MP2, MP3, MP4, CCD, CCSD, CID, CISD, QCISD, QCISD(T), and CASSCF levels of theory with the 3-21G, 6-31G**, 6-311++G**, and D95++(3df,2p) basis sets. The UHF, MP4, CIS, CISD, CCSD, QCISD, QCISD(T), and CASSCF levels of theory predict the transition state to be a highly bent C_{2v} symmetry structure, whereas MP2, MP3, and CCD levels predict the C_{2v} symmetry structure to be a shallow minimum bound by up to 0.4 kcal/mol. The MP2/6-31G** C_{2v} structure is bracketed by two C_s symmetry transition states with bond lengths of 1.1411 and 1.0541 Å and a bond angle of 127.0°. The C_{2v} minimum on the MP2, MP3, and CCD surfaces is caused by inadequately treated avoided crossings between the bond making/breaking state and two broken symmetry F + HF hydrogen bonding states. Dynamic correlation methods that include single excitations in an interative or self consistent manner, such as CASSCF, CISD, CCSD, and QCISD, appear to treat the avoided crossings properly and predict a suitable transition state. At the QCISD(T)/D95++(3df,2p) level, the C_{2v} transition state geometry is R(H–F) = 1.102 Å and ∠F–H–F = 134.6° and the reaction barrier is 17.5 kcal/mol.

Introduction

Hydrogen atom abstraction reactions, XH + Y → X + HY, are of general interest because of their importance in radical chemistry and combustion processes. Recently, hydrogen exchange reactions with X, Y = halogen have generated considerable interest in connection with transition state spectroscopy.[1] Under favorable circumstances, photodetachment of an electron from a bihalide anion, XHY^-, can lead to a neutral species with a geometry similar to the transition state for the reaction XH + Y → X + HY. Neumark et al.[2-5] found structure in the photodetachment spectra of $ClHCl^-$, $BrHBr^-$, and IHI^-, suggesting the existence of vibrational resonances near the transition state. Higher resolution experiments[5] showed secondary structure in the IHI^- spectrum. Schatz[6] and Bowman[7] have published detailed quantum scattering calculations and find reasonable agreement with the experimental photodetachment spectra. Morokuma[8] has suggested that the $^2\Pi$ state could also be contributing to the observed spectra. In contrast to these systems, Neumark[9] found no structure in the photoelectron detachment spectrum of FHF^-. Ault and Andrews[10] have shown that earlier attempts[11] to isolate a symmetric, quasistable XHX complex by matrix isolation produced bihalide ions rather than the neutral species. Thus, there is no experimental evidence for a symmetric FHF complex and no indication of any vibrational resonances in FHF for geometries similar to FHF^-.

In early calculations, Schaefer et al.[12] and Peyerimhoff et al.[13] obtained barrier heights for collinear F + HF by Hartree–Fock theory and configuration interaction. Vibrational frequency calculations by LeRoy et al.[14] showed the F + HF transition state to be linear at the HF/4-31G level. More recently, VB-SCF and CAS-SCF calculations[15] have been used to probe the origin of the barrier for collinear F + HF. There appears to be no high level molecular orbital studies on non-collinear F + HF in the recent literature. Calculations on other X + HY abstraction reactions have demonstrated that some of these transition states are bent. For example, for X = Y = Cl, POL-CI calculations yielded an optimized bond angle of approximately 160°.[16] The bending is sometimes revealed only when extensive electron correlation corrections are included. The transition state for the F + H_2 reaction is linear at the HF level but has an angle of approximately 120°[17] when a large multi-reference CI approach is employed (however, the potential energy surface is extremely flat with respect to the bending motion). At the highest level of calculations carried out, QCISD(T)/D95++(3df,2p), the F + HF transition state was found to be strongly bent with an angle of 135°.

During a series of investigations of barriers for hydrogen abstraction in X + HY,[18] XCH_2 + HY,[19] and XCH_2 + HCH_2Y[20] (X, Y = H, F, Cl, OH, SH, CN), some unusual features were noted and prompted a study of the structure and energetics of the F + HF reaction at levels of theory higher than Hartree–Fock. Of the various methods for including electron correlation, second-

† Present address: Sandoz Research Institute, 59 Route 10, East Hanover, NJ 07936.

(1) Zewail, A. H.; Bernstein, R. B. *Chem. Eng. News* **1988**, *66*(*45*), 24.
(2) Metz, R. B.; Kitsopoulos, T.; Weaver, A.; Neumark, D. M. *J. Chem. Phys.* **1988**, *88*, 1463.
(3) Weaver, A.; Metz, R. B.; Bradforth, S. E.; Neumark, D. M. *J. Phys. Chem.* **1988**, *92*, 5558.
(4) Metz, R. B.; Weaver, A.; Bradforth, S. E.; Kitsopoulos, T. N.; Neumark, D. M. *J. Phys. Chem.* **1990**, *94*, 1377.
(5) Waller, I. M.; Kitsopoulos, T. N.; Neumark, D. M. *J. Phys. Chem.* **1990**, *94*, 2240.
(6) Schatz, G. C. *J. Phys. Chem.* **1990**, *94*, 6157.
(7) Gazdy, B.; Bowman, J. M. *J. Chem. Phys.* **1989**, *91*, 4615. Bowman, J. M.; Gazdy, B. *J. Phys. Chem.* **1989**, *93*, 5129.
(8) Yamashita, K.; Morokuma, K. *J. Chem. Phys.* **1990**, *93*, 3716; **1990**, *94*, 831.
(9) Neumark, D. M. Private communication.
(10) Ault, B. S.; Andrews, L. *J. Am. Chem. Soc.* **1975**, *97*, 3825. Ault, B. S. *J. Chem. Phys.* **1978**, *68*, 4012. McDonald, S. A.; Andrews, L. *J. Chem. Phys.* **1979**, *70*, 3134.
(11) Noble, P. N.; Pimentel, G. C. *J. Chem. Phys.* **1968**, *49*, 3165. Milligan, D. E.; Jacox, M. E. *J. Chem. Phys.* **1970**, *53*, 2034; **1971**, *55*, 2550. Bondebey, V. E.; Pimentel, G. C.; Noble, P. N. *J. Chem. Phys.* **1971**, *55*, 540.
(12) O'Neil, S. V.; Schaefer, H. F., III; Bender, C. F. *Proc. Natl. Acad. Sci. U.S.A.* **1974**, *71*, 104.
(13) Pruess, R.; Peyerimhoff, S. D.; Buenker, R. J. *J. Mol. Struct.* **1977**, *40*, 117.
(14) LeRoy, G.; Sana, M.; Tinant, A. *Can. J. Chem.* **1985**, *63*, 1447.
(15) Benneyworth, P. B.; Balint-Kurti, G. G.; Davis, M. J.; Williams, I. H. *J. Phys. Chem.* **1992**, *96*, 4346.
(16) Garrett, B. C.; Truhlar, D. G.; Wagner, A. F.; Dunning, T. H., Jr. *J. Chem. Phys.* **1983**, *78*, 4400.
(17) Bauschlicher, C. W.; Walch, S. P.; Langhoff, S. R.; Taylor, P. R.; Jaffe, R. L. *J. Chem. Phys.* **1988**, *88*, 1743.
(18) Fox, G. L.; Schlegel, H. B. In preparation.
(19) Ayala, P. Y.; Fox, G. L.; Schlegel, H. B. In preparation.
(20) Fox, G. L.; Schlegel, H. B. *J. Phys. Chem.* **1992**, *96*, 298.

0002-7863/93/1515-6870$04.00/0

Table I. Total Energies (au) and Relative Energies (kcal/mol) for Reactants and Transition States

level	F	HF	FHF	ΔE_{rel}[a]
UHF/3-21G	-98.845 009	-99.460 219	-198.258 790	29.14
MP2/3-21G	-98.925 143	-99.583 882	-198.478 227	19.33
QCISD(T)/3-21G	-98.928 312	-99.586 615	-198.491 931	14.43
UHF/6-31G**	-99.364 957	-100.011 691	-199.312 236	40.42
UMP2/6-31G** C_{2v}[b]	-99.489 039	-100.196 700	-199.654 463	19.63
UMP2/6-31G** C_s			-199.653 792	20.05
UMP3/6-31G**	-99.495 693	-100.196 402	-199.655 351	23.06
UMP4SDTQ/6-31G**	-99.498 652	-100.201 430	-199.669 626	19.11
CAS(3,3)/6-31G**			-199.338 988	
CAS(7,6)/6-31G**			-199.365 898	
CID/6-31G**	-99.494 370	-100.193 942	-199.636 709	32.38
CISD/6-31G**	-99.495 124	-100.194 892	-199.645 162	28.15
CCD/6-31G**	-99.497 088	-100.198 186	-199.658 350	23.17
CCSD/6-31G**	-99.497 681	-100.199 009	-199.666 825	18.74
QCISD/6-31G**	-99.497 954	-100.199 384	-199.668 535	18.07
QCISD(T)/6-31G**	-99.498 983	-100.201 279	-199.673 855	16.57
UHF/6-311++G**	-99.399 893	-100.053 305	-199.383 339	43.84
UMP2/6-311++G**	-99.578 265	-100.297 937	-199.836 739	24.76
CCD/6-311++G**	-99.568 610	-100.279 123	-199.803 868	27.53
CCSD/6-311++G**	-99.569 512	-100.280 786	-199.814 288	22.60
QCISD(T)/6-311++G**	-99.571 685	-100.285 333	-199.825 901	19.53
UHF/D95++(3df,2p)	-99.400 961	-100.054 980	-199.386 244	43.73
UMP2/D95++(3df,2p)	-99.591 190	-100.317 007	-199.872 355	22.49
CCD/D95++(3df,2p)	-99.588 611	-100.305 112	-199.852 738	25.72
QCISD(T)/D95++(3df,2p)	-99.593 039	-100.312 099	-199.877 304	17.47
PMP2/6-31G**//UMP2/6-31G**	-99.488 228	-100.196 700	-199.655 018	18.77
PMP3/6-31G**//UMP3/6-31G**	-99.496 116	-100.196 402	-199.659 655	20.62
PMP4SDTQ/6-31G**//UMP4/6-31G**	-99.499 075	-100.201 430	-199.673 973	16.65

[a] ΔE_{rel} is the same as the reaction barrier, ΔE^*, for all cases except at the UMP2 and CCD levels. [b] The well depth at the UMP2/6-31G** level is 0.42 kcal/mol.

order Møller–Plesset perturbation theory, MP2, is used most frequently because of its relatively low computational cost and the availability of energy derivatives. As will be shown below, the F + HF transition state is one of a small number of cases where MP2 theory is qualitatively incorrect. It is the aim of this paper to understand the detailed origin of this problem.

Methods Section

Ab initio molecular orbital calculations were carried out using the GAUSSIAN series of programs.[21] The 3-21G, 6-31G**, 6-311++G**, and D95++(3df,2p) basis sets[22] were employed to optimize the geometries of the reactants and transition states using Hartree–Fock theory (HF), Møller–Plesset perturbation theory (MP2, MP3, MP4DQ, MP4SDQ, MP4SDTQ), configuration interaction (CID, CISD), coupled clusters methods (CCD, CCSD), and quadratic configuration interaction [QCISD, QCISD(T)], and complete active space multi-configuration self consistent field theory (CASSCF). Analytical gradient techniques[23] were used for optimization with spin unrestricted HF, MP2, CID, CISD, QCISD, and CAS-SCF levels of theory and a modified Fletcher–Powell optimization method[24] for the CCD, CCSD, MP3, MP4SDTQ, and QCISD(T) levels of theory. Total energies are listed in Table I and optimized geometries are given in Table II. Some calculations were also carried out with wave functions that are eigenfunctions of spin: complete active space multi-configuration SCF (CASSCF), restricted open shell Hartree–Fock (ROHF), and restricted open shell second-order Møller–Plesset perturbation theory[25] (ROMP2). The stationary points on the potential energy surfaces were characterized by vibrational frequency calculations (Table III). Second derivatives were calculated analytically at the Hartree–Fock level,[26] by numerical differentiation of analytical gradients for the MP2, CID, CISD, QCISD, and CAS-SCF levels, and by double numerical differentiation of the energy with respect to nuclear coordinates for the MP3, MP4SDTQ, and QCISD(T) levels of theory. The MP2 calculations were performed using all of the occupied and virtual orbitals. For all of the other methods of correlation, the frozen core approximation was employed for the geometry optimizations and frequency calculations. Energy-only calculations at all levels of electron correlation corrections include all orbitals (i.e. not frozen core).

Table II. Geometries of F–H–F[a]

level	R(H–F)	∠F–H–F
UHF/3-21G	1.1277	180.0
MP2/3-21G	1.1126	127.7
QCISD(T)/3-21G	1.1419	123.6
UHF/6-31G**	1.0943	151.5
UMP2/6-31G** C_{2v}	1.0873	126.1
UMP2/6-31G** C_s	1.0541, 1.1411	127.0
UMP3/6-31G**	1.0896	129.6
UMP4SDTQ/6-31G**	1.0957	127.1
CAS(3,3)/6-31G**	1.1140	180.0
CAS(7,6)/6-31G**	1.1110	128.7
CID/6-31G**	1.0884	131.5
CISD/6-31G**	1.0933	130.7
CCD/6-31G**	1.0913	129.9
CCSD/6-31G**	1.1050	128.6
QCISD/6-31G**	1.1064	128.3
QCISD(T)/6-31G**	1.1089	127.1
UHF/6-311++G**	1.0907	165.6
UMP2/6-311++G**	1.0771	135.5
CCD/6-311++G**	1.0819	141.8
CCSD/6-311++G**	1.0952	139.1
QCISD(T)/6-311++G**	1.0999	137.4
UHF/D95++(3df,2p)	1.0948	164.4
UMP2/D95++(3df,2p)	1.0800	130.5
CCD/D95++(3df,2p)	1.0846	136.4
QCISD(T)/D95++(3df,2p)	1.1023	134.6

[a] Bond lengths in Å and angles in deg.

Discussion

Inspection of the geometries summarized in Table II shows that the transition states calculated at levels of theory other than

(21) Frisch, M. J.; Head-Gordon, M.; Trucks, G. W.; Foresman, J. B.; Schlegel, H. B.; Raghavachari, K.; Robb, M. A.; Binkley, J. S.; Gonzalez, C.; Defrees, D. J.; Fox, D. J.; Whiteside, R. A.; Seeger, R.; Melius, C. F.; Baker, J.; Martin, R. L.; Kahn, L. R.; Stewart, J. J. P.; Topiol, S.; Pople, J. A.; Gaussian 90, Revision H, 1990, Gaussian, Inc.: Pittsburgh, PA.

(22) Huzinaga, S. *J. Chem. Phys.* **1965**, *42*, 1293. Hehre, W.; Radom, L.; Schleyer, P. v. R.; Pople, J. A. *Ab Initio Molecular Orbital Theory*; Wiley, New York, 1986; note that 6-31G** and 6-31G(d,p) are synonymous.

(23) Schlegel, H. B. *J. Comput. Chem.* **1982**, *3*, 214.

(24) Collins, J. B.; Schleyer, P. v. R.; Binkley, J. S.; Pople, J. A. *J. Chem. Phys.* **1976**, *64*, 5142.

(25) Knowles, J. P.; Andrews, J. F.; Amos, R. D.; Handy, N. C.; Pople, J. A. *Chem. Phys. Lett.* **1991**, *186*, 130. Amos, R. D.; Andrews, J. F.; Handy, N. C.; Knowles, J. F. *Chem. Phys. Lett.* **1991**, *185*, 256.

(26) Pople, J. A.; Schlegel, H. B.; Krishnan, R.; Defrees, D. J.; Binkley, J. S.; Frisch, M. J.; Whiteside, R. A.; Hout, R. F.; Hehre, W. J. *Int. J. Quantum Chem. Symp.* **1981**, *15*, 269.

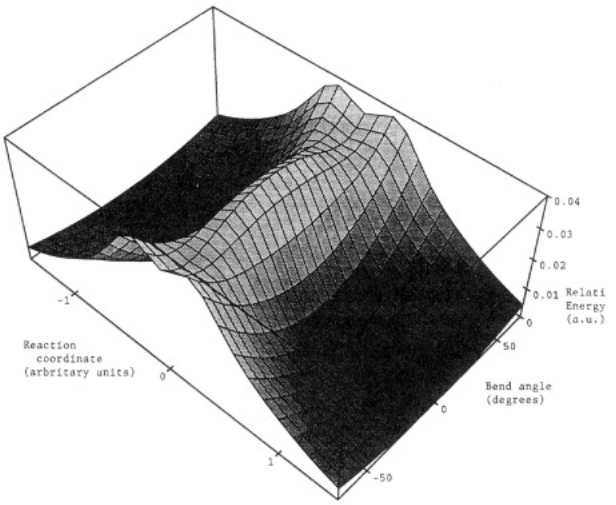

Figure 1. Model potential energy surface for F + HF fitted to selected MP2/6-31G** energies and derivatives (bending coordinate is in degrees from linearity).

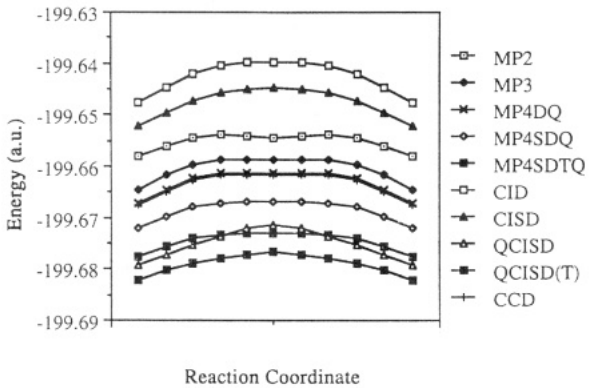

Figure 2. Potential energy curves at various levels of theory along an approximate MP2/6-31G** reaction path.

Table III. Vibrational Frequencies for F–H–F[a]

level	ν_1	ν_2	ν_3
UHF/3-21G $D_{\infty h}$	4322i	272(2)	560
MP2/3-31G	3294i	322	1911
UHF/6-31G**	5960i	277	1162
UMP2/6-31G** C_{2v}	493	2074	3134
UMP2/6-31G** C_s	3404i	445	2009
UMP4SDTQ/6-31G**	398i	472	1978
CAS(3,3)/6-31G** $D_{\infty h}$	4732i	287(2)	580
CAS(7,6)/6-31G**	9603i	474	1752
CID/6-31G**	1399i	436	1870
CCD/6-31G**	449	1913	2098
QCISD(T)/6-31G**	1891i	472	1848
UHF/6-311++G**	6292i	235	788
UMP2/6-311++G**	447	1800	1906
UHF/D95++(3df,2p)	2677i	204	820
UMP2/D95++(3df,2p)	428	1895	4548

[a] In cm^{-1}.

UHF/3-21G and CAS(3,3)/6-31G** are significantly bent. The bond angle at the UHF/6-31G** level is 151°, and at correlated levels of theory other than CAS(3,3), the angle lies in the range of 126–142°. The calculated barriers are ca. 40 kcal/mol at the Hartree–Fock level and 15–30 kcal/mol when electron correlation corrections are included. The highest levels of theory employed are in agreement that the transition state geometry is of C_{2v} symmetry with bond lengths of 1.09 ± 0.01 Å and a bond angle of 132 ± 5°. However, the corresponding MP2, MP3, and CCD potential energy surfaces have a small depression centered at the C_{2v} geometry bracketed by transition states of C_s symmetry. The whimsical term "Lake Eyring" has occasionally been used in the vernacular to refer to such a complex or basin in the region of a transition state. For basis sets of 6-31G** quality or better, the minimum at the MP2 level appears to be independent of the quality of basis set. The main focus of this paper is to gain an understanding of the origin of this anomaly.

An approximate potential energy surface has been fit to the energies, gradients, and second derivatives at a suitable set of points computed at the MP2/6-31G** level. As can readily be seen in Figure 1, this surface has a shallow depression along the reaction path centered at the C_{2v} geometry. Such a characteristic in the surface, if it were real and not an artifact of the theoretical method, would lead to intense interest in both the experimental and theoretical communities to detect the quasistable intermediate and probe the effects of such a minimum on the dynamical behavior. However, as mentioned above, this minimum is not reproduced at higher levels of theory and is an artifact of Møller–Plesset perturbation theory.

To investigate the source of this shallow well, the C_{2v} structure of F–H–F was optimized at various levels of theory and characterized by frequency calculations at the same level. The total energies of the reactants, intermediate (at the levels where it exists), and transition states are listed in Table I. The potential energy surfaces at the MP2, MP3, and CCD levels of theory with the 6-31G**, 6-311++G**, and D95++(3df,2p) basis sets exhibit the spurious minima; however, with smaller basis sets (STO-3G, 3-21G, and 4-31G) the spurious minimum does not exist. At the CID, CISD, MP4SDTQ, QCISD, QCISD(T), and CAS-SCF levels of theory with all of the basis sets considered, the optimized C_{2v} structure is a true transition state with one imaginary frequency.

To analyze the effect of the level of theory on the shape of the potential energy surface, a number of calculations were performed along an approximate reaction path obtained from the MP2/6-31G** calculations. Eleven points along the MP2/6-31G** reaction path were chosen: the MP2/6-31G** optimized C_{2v} symmetry intermediate, the MP2/6-31G** optimized C_s transition states, a linear interpolated point midway between the C_{2v} intermediate and each transition state, and three linearly extrapolated points beyond each transition state. The energy profiles calculated with the 6-31G** basis set using a variety of electron correlation methods are depicted in Figure 2. The MP2, MP3, MP4DQ, and CCD energy profiles exhibit the spurious minima, whereas the MP4SDQ and MP4SDTQ levels predict the surface to be extremely flat and UHF, CID, CISD, QCISD, and QCISD(T) levels all agree that there is a single transition state along the reaction coordinate.

The first conclusion that one might jump to is that an excited state strongly interacts with the ground state, i.e. sizable nondynamic correlation effects. Perturbation theory handles strong interactions poorly and might lead to the anomalous depression, whereas variational methods treat the interaction properly and reproduce the correct topology of the potential energy surface. This hypothesis can be probed by a simple two-state model. Two limiting cases have been considered: (a) the two states are chosen to have a quadratic dependence on the reaction path and are allowed to interact via a constant matrix element and (b) the energy difference between the two states is fixed and the interaction matrix element is allowed to be quadratic:

$$\begin{bmatrix} E_1 & H_{12} \\ H_{12} & E_2 \end{bmatrix}\begin{bmatrix} C_1 \\ C_2 \end{bmatrix} = E_{\text{corr}}\begin{bmatrix} C_1 \\ C_2 \end{bmatrix} \quad (1)$$

Case (a): $E_1 = a + bs^2$, $E_2 = c + ds^2$, $H_{12} = 0.01$

Case (b): $E_1 = a + bs^2$, $E_2 = E_1 + 0.003$, $H_{12} = c + ds^2$

In both cases the constants, a–d, are determined by fitting the second-order perturbation energy of the two-state system to the ab initio UMP2 energy at seven points along the approximate reaction path. As shown in Figure 3a the choice of $H_{12} = 0.01$

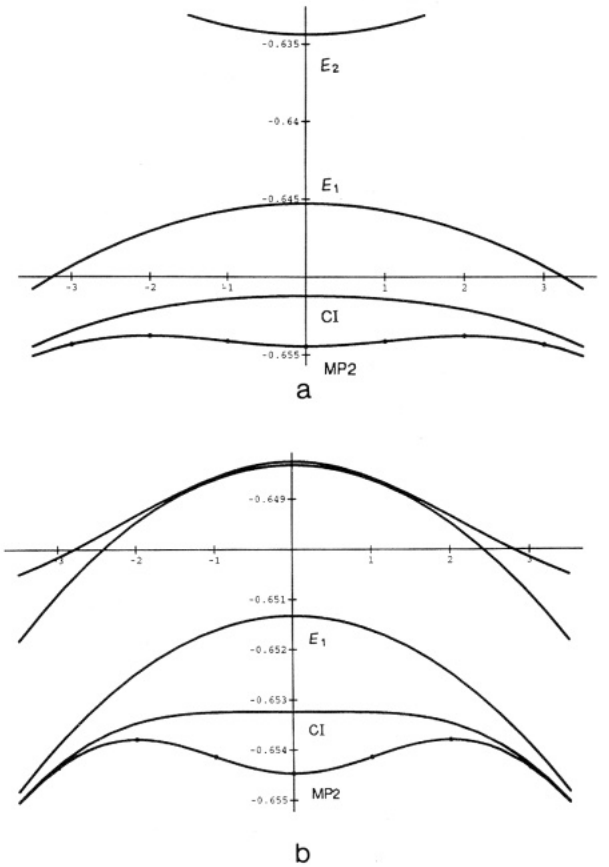

Figure 3. Simple two-state model potential energy curves, eq 3, for case (a) with quadratic ground and excited states and constant interaction matrix element ($H_{12} = 0.01$) and case (b) with constant energy difference ($\Delta E = 0.003$) and quadratic interaction matrix element.

au for case (a) yields a model system in which the second-order perturbation energy has a local minimum at the symmetric structure but the variational energy (CI energy) does not. Likewise Figure 3b demonstrates that the corresponding situation can be obtained for case (b) with $\Delta E = 0.003$ au. Therefore, these simple two-state models suggest that the behavior of the UMP2 surface for F + HF could be due to a strong interaction with a low-lying excited state.

To see which interactions could be causing the problems with the MP2 surface, the individual molecular orbitals and their contributions to the correlation energy were examined in more detail. As can be seen in Figure 4, the occupied orbitals involved in the forming and breaking H–F bonds are 5 and 8 from the α set and 5 from the β set. Note that the in-plane lone pairs on the fluorines mix strongly with the H–F bonding orbitals giving rise to orbital 9β (the in-plane α lone pairs are relatively unperturbed). The corresponding virtual orbitals related to the H–F bond breaking are 11α, 12α, 10β, 11β, and 12β.

The contributions to the correlation energy can be partitioned into a sum of pair energies.

$$E_{\text{corr}} = \sum_{i,j}^{i \neq j} \epsilon_{ij} \qquad (2)$$

In the region of the transition state the most important components of the changes in the correlation energy should come from the orbitals involved in the bond making and breaking. Let E'_2 be the contribution of the $(5\alpha,8\alpha)$, $(5\alpha,5\beta)$, $(5\alpha,9\beta)$, $(8\alpha,5\beta)$, $(8\alpha,9\beta)$, and $(5\beta,9\beta)$ pair energies. It can be seen from Figure 5 that E'_2 is in fact the major contributor to the spurious minimum along the MP2 reaction path and that the remainder of the correlation energy, $E_2 - E'_2$, is nearly constant in this region. The contributions to E'_2 can be further decomposed by examining which excitations contribute most strongly to the E'_2. Let E''_2

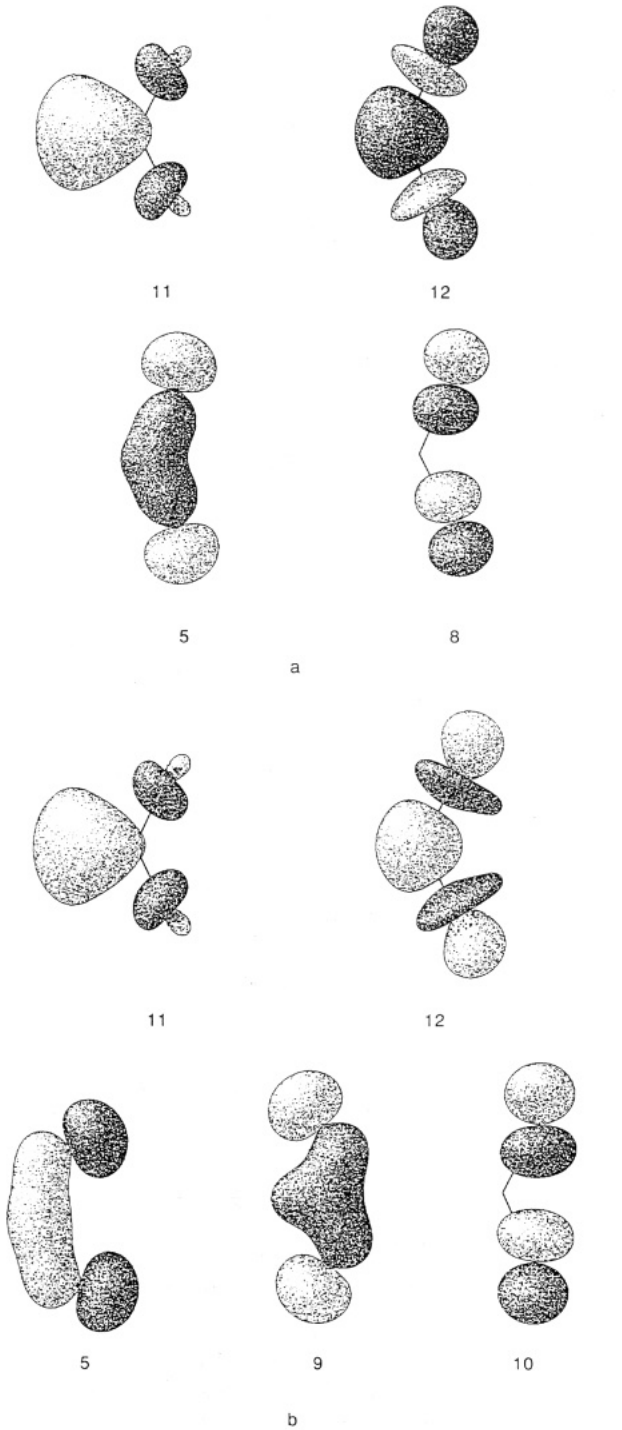

Figure 4. Molecular orbitals involved in the bond making/breaking process: (a) α MO's, (b) β MO's.

be the contributions from the symmetry allowed excitations in the active space of the 5, 8, 11, and 12 α orbitals and 5, 9, 10, 11, and 12 β orbitals. Figure 6 shows that the excitations in E''_2 account for approximately 90% of the dip in E'_2 along the reaction path.

The key contributions to the CID and QCISD correlation energy are defined similar to the MP2 term and are shown in Figure 7. The CID and QCISD contributions mimic the MP2 contribution. The stabilizing effects of the interactions included in E'_2 are, no doubt, responsible for the flattening of the potential energy surface near the C_{2v} symmetry structure. However, since the differences between the MP2 E'_2 and the CID or QCISD contributions remain nearly constant along the reaction path, this simple explanation cannot be solely responsible for the spurious minimum.

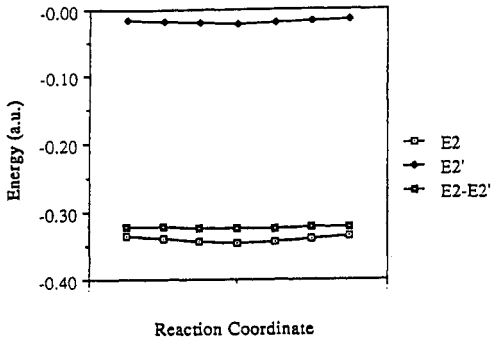

Figure 5. Second-order correlation energy, E_2, contributions from (5α,8α), (5α,5β), (5α,9β), (8α,5β), (8α,9β), and (5β,9β) pair energies, E'_2, and their difference along the approximate MP2/6-31G** reaction path.

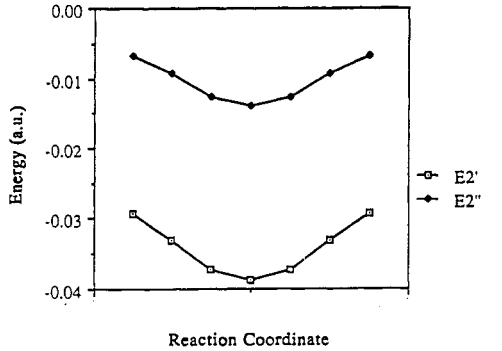

Figure 6. Pair energy, E'_2, and correlation contributions, E''_2, from orbitals 5α, 8α, 11α, 12α, 5β, 9β, 10β, 11β, and 12β along the approximate MP2/6-31G** reaction path.

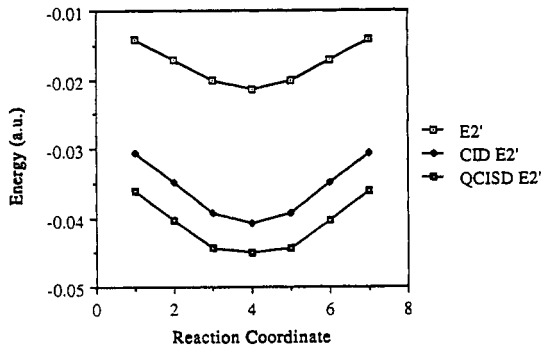

Figure 7. Pair energy calculated at the MP2, CID and QCISD levels along the approximate MP2/6-31G** reaction path.

The fourth-order perturbation expansion with only double and quadruple excitations, MP4DQ, exhibits similar behavior to the MP2 potential energy surface, but the addition of single excitations (MP4SDQ) or single and triple excitations (MP4SDTQ) removes the spurious minima along the reaction coordinate. However, the resulting surfaces remain extremely flat near the C_{2v} transition state. This is in contrast to the more accurate correlated levels and shows that even the fourth-order perturbation expansion is inadequate for this reaction.

Another potential source of problems with unrestricted Møller–Plesset perturbation theory is spin contamination. Substantial spin contamination can cause errors of 5–15 kcal/mol in barrier heights.[27] Thus, a second working hypothesis is that spin contamination is the source of the anomaly. Spin projection can be used to remove the effects of the unwanted spin states. As can be seen from Figure 8, spin projection deepens the well when cross sections at the PMPn levels are compared to the UMPn

(27) Schlegel, H. B. *J. Chem. Phys.* **1986**, *84*, 4530. Schlegel, H. B. *J. Phys. Chem.* **1988**, *92*, 3075. Sosa, C.; Schlegel, H. B. *J. Am. Chem. Soc.* **1987**, *109*, 4193, 7007. Schlegel, H. B.; Sosa, C. *Chem. Phys. Lett.* **1988**, *145*, 329.

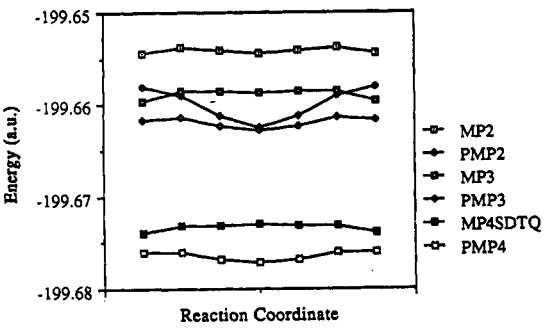

Figure 8. Spin projected MPn potential energy curves along the approximate MP2/6-31G** reaction path.

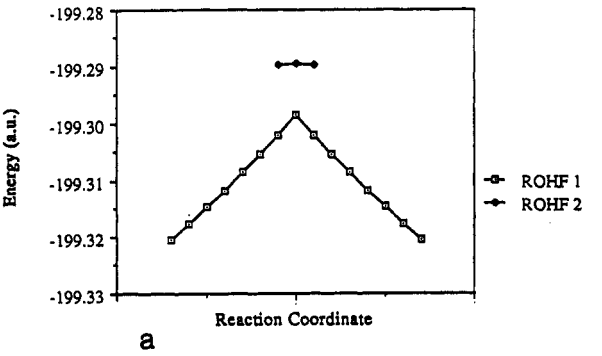

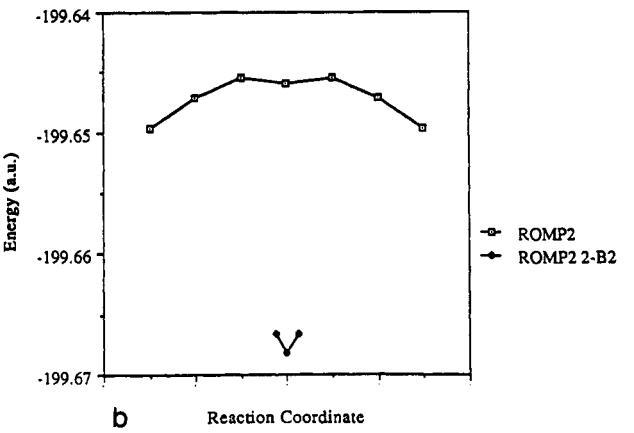

Figure 9. Potential energy curves calculated at (a) ROHF/6-31G** and (b) ROMP2/6-31G** along the approximate MP2/6-31G** reaction path. Note that the upper ROHF state corresponds to the lower ROMP2 state.

levels (tempting one to conclude that spin projection does not work, but see below). An alternate way to overcome the problems of spin contamination in the unrestricted Møller–Plesset perturbation theory is to use a restricted open shell (ROHF) reference wave function and include electron correlation corrections by restricted open shell MP2 theory (ROMP2).[25] The ROHF and ROMP2 energy profiles are shown in Figure 9. The ROHF ground state wave function has broken spatial symmetry. The corresponding ROMP2 potential energy curve is higher than the UMP2 curve and also shows a less pronounced well centered around the C_{2v} symmetry structure. The spatially symmetric $^2B_2$ ROHF state at the C_{2v} geometry lies above the crossing of the broken symmetry states. The corresponding ROMP2 energy is substantially lower than the broken symmetry ROMP2 energy curve. In fact, the $^2B_2$ ROMP2 energy is similar to the projected UMP2 (PMP2) energy for the C_{2v} structure, indicating that spin projection is changing the energy in the correct direction. The $^2B_2$ ROHF and ROMP2 surfaces, however, can be followed for

Scheme I

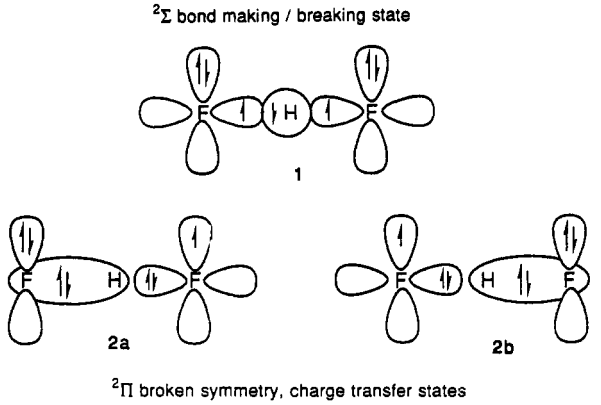

only a short distance from the C_{2v} structure before SCF convergence problems become overwhelming. Since the shallow well persists with a reference wave function free of spin contamination, spin contamination cannot be the source of the anomalous behavior of the MP2 surface. Because of symmetry breaking, the ROHF and ROMP2 approaches do not provide a satisfactory way around the UMP2 difficulties. Nevertheless, the presence of the broken symmetry states suggests a re-examination of the UHF surface for analogous states.

The origin of the broken symmetry states can be seen best by examining the linear structure. The three σ orbitals involved in the making and breaking of the bonds and the π lone pairs are sketched in Scheme I. The spatially symmetric configuration has the expected three σ electrons and is denoted structure **1**, while the two broken symmetry configurations can be formed by removing an electron from the π lone pair of one fluorine atom and placing it into the σ orbitals. The σ orbitals can localize into an H–F bond and a fluorine σ lone pair that interact via a hydrogen bond (structure **2a**). The complementary broken symmetry state, structure **2b**, is formed by taking the electron from the other fluorine atom. At the linear geometry the σ state and the broken symmetry π states cannot interact. As can be seen in Figure 10, the curves cross and the broken symmetry π states become lower for an antisymmetric displacement of 0.05 Å.

The correlation corrections calculated at the MP2 level are quite different for the symmetric state and the two broken symmetry states (see Figure 10b). Not surprisingly, the symmetric state that describes the making and breaking of the σ bonds has a larger value of E_2; the broken symmetry states describe an elongated H–F bond hydrogen bonded to a lone pair of the other fluorine and have a significantly smaller E_2. In the linear geometry, the states are of different symmetry, hence there is no difficulty arising from an avoided crossing.

When the linear structure is bent the four broken symmetry π states split into two groups: one pair has the odd electron in a plane perpendicular to the FHF nuclear framework plane (A'' state in C_s point group) and the other pair has the odd π electron in the plane (A' state in C_s point group). The A' states are of the same symmetry as the ground state and can interact with it. At an angle of 165° and antisymmetric bond length displacements of 0.05 Å or greater, the ground state UHF wave function is dominated by the broken symmetry wave function. The MP2 electron correlation energy is greater for the bond making/breaking state than for the broken symmetry state as can be seen in Figure 11b. With a small amount of bending the crossing between the two UHF states is weakly avoided and the transition from the strongly correlated state **1** to the less correlated state **2** is abrupt. As bending increases the interaction becomes larger and the transition becomes smoother until all that remains is two small bumps separated by a small depression; this is depicted in Figure 12. *This is the origin of the shallow depression on the MP2 surface.* The increased interaction for the nonlinear geometry lowers the energy and hence is responsible for the bent geometry of the transition state. The strong interactions between

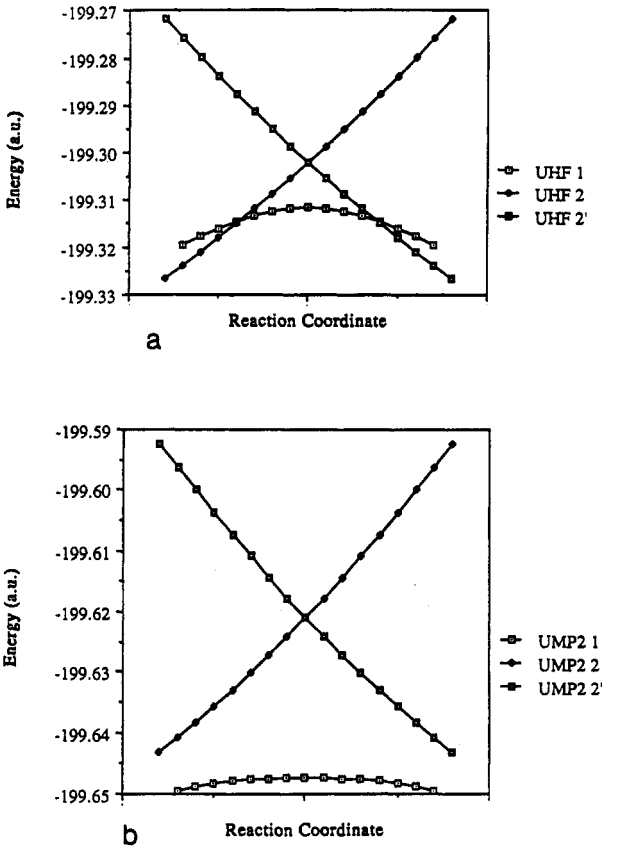

Figure 10. Potential energy curves calculated at (a) UHF/6-31G** and (b) UMP2/6-31G** along a collinear MP2/6-31G** reaction path.

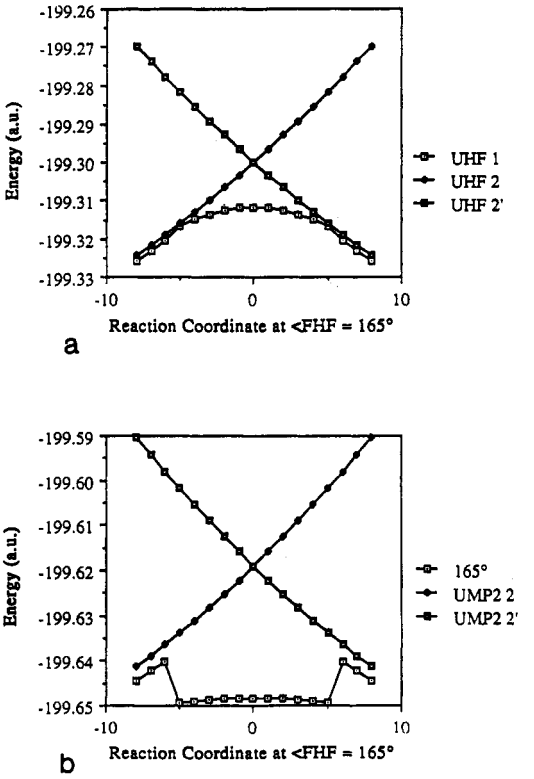

Figure 11. Potential energy curves calculated at (a) UHF/6-31G** and (b) UMP2/6-31G** along a reaction path with the F–H–F angle fixed at 165°.

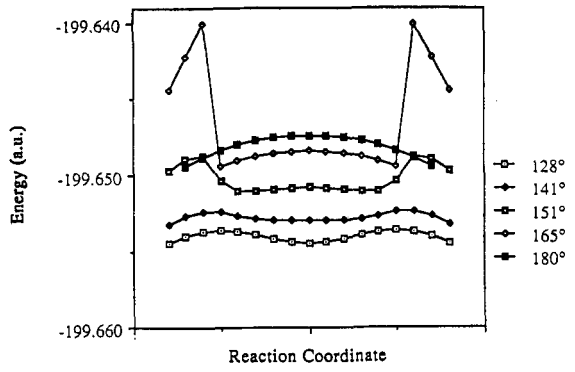

Figure 12. Potential energy curves calculated at the UMP2/6-31G** level along a reaction path with the F–H–F angle fixed at various values.

state **1** and state **2** suggest that a proper treatment of the electronic structure of this system may require CAS-SCF.

States **1** and **2** formally differ by a single excitation (Scheme I). The CISD, QCISD, QCISD(T), and CCSD calculations appear to handle this interaction properly. However, the MP2, MP3, and CCD methods which do not include single excitations perform rather poorly. The proper means of handling strong interactions between states, i.e. non-dynamic correlation, is multi-configuration SCF. A small CAS-SCF/6-31G** calculation capable of describing the H–F bond making and breaking process would include 3 electrons in 3 orbitals: σ bonding (σ), sigma nonbonding (σ^{nb}), and σ antibonding (σ^*) (corresponding to orbitals 5, 9, and 11 in Figure 4a). With the 6-31G** basis set the 3 electron 3 orbital CAS-SCF yielded a linear $D_{\infty h}$ transition state. However, a larger CAS-SCF/6-31G** calculation with 7 electrons and including the occupied and unoccupied in-plane π and π^* lone pair-like orbitals along with the σ, σ^{nb}, and σ^* orbitals yielded a highly bent C_{2v} symmetry transition state ($\angle$FHF = 132°). Both CAS-SCF structures have one imaginary frequency, indicating they are true transition states. The agreement between the large CAS-SCF calculation and the QCI, CID, CISD, and CCSD transition states indicates that these methods are sufficient to handle the interaction with the broken symmetry states, whereas MPn and CCD levels of theory are not.

(28) For leading references to the interpretation of the anomeric effect, see: Wolfe, S.; Whangbo, M.-H.; Mitchell, D. *J. Carbohydr. Res.* **1979**, *69*, 1.

Secondly, the CASSCF calculations show that the bending in the transition is due to the interaction of the fluorine lone pairs with the partially formed/broken H–F σ bonds. This type of interaction is normally termed hyperconjugation and is better known for its conformational effects in ground state molecules (e.g. the anomeric effect[28]).

The highly bent nature of the F + HF transition state is probably the reason that no structure is seen in the photodetachment spectra of FHF^-. The FHF^- ion is linear and would have very poor Frank–Condon overlap with the highly bent F–H–F transition state. By contrast, the Cl–H–Cl transition state is closer to linear and has good overlap with $Cl–H–Cl^-$, giving rise to the observed spectral features.[2]

Conclusion

The transition state for F + HF was found to be a highly bent, C_{2v} structure (R(HF) = 1.102 Å, $\angle$F–H–F = 134.6 Å, E_{rel} = 17.5 kcal/mol at the QCISD(T)/D95 ++ (3df,2p) level). The MP2/6-31G** potential energy surface contains a disturbing anomaly: instead of a transition state at C_{2v} geometry, one finds a shallow depression. At higher levels of theory, this artifact disappears. The weakly bound complex at the MP2 level is not the result of a strong interaction with a higher state at the C_{2v} geometry, nor is it the result of spin contamination. The source of the problem lies with the pair of C_s transition states that flank the C_{2v} complex at the MP2 level. These are residuals of avoided crossings between the bond making/breaking state and two broken symmetry, hydrogen bonding states. These broken symmetry states are formally single excitations from a fluorine lone pair into the σ non-bonding orbital. Higher levels of calculation that include single excitations in an iterative or self consistent fashion, rather than perturbative, treat this avoided crossing properly and thus do not have anomalous C_s transition states and a C_{2v} minimum. The strong stabilizing interactions (i.e., hyperconjugation) between the fluorine lone pairs and the σ orbitals involved in bond making/breaking are also responsible for the highly bent geometry of the transition structure.

Acknowledgment. We would like to thank the National Science Foundation for financial support (Grant No. CHE 90-20398) and the Pittsburgh Supercomputing Center and Cray Research for generous grants of computer time.